Supplementary Files to ‘Insights into temporal earthquake clustering from the Settlement Fault, southeastern Otago, Aotearoa New Zealand’

Contents:

- Supplement S1: Supplementary figures to the main manuscript (Figures S1-S8)
- Supplement S2: Laboratory report for the Owaka Trench radiocarbon dating samples
- Supplement S3: Laboratory report for the Owaka Trench OSL samples

Supplement S1

Figure S1

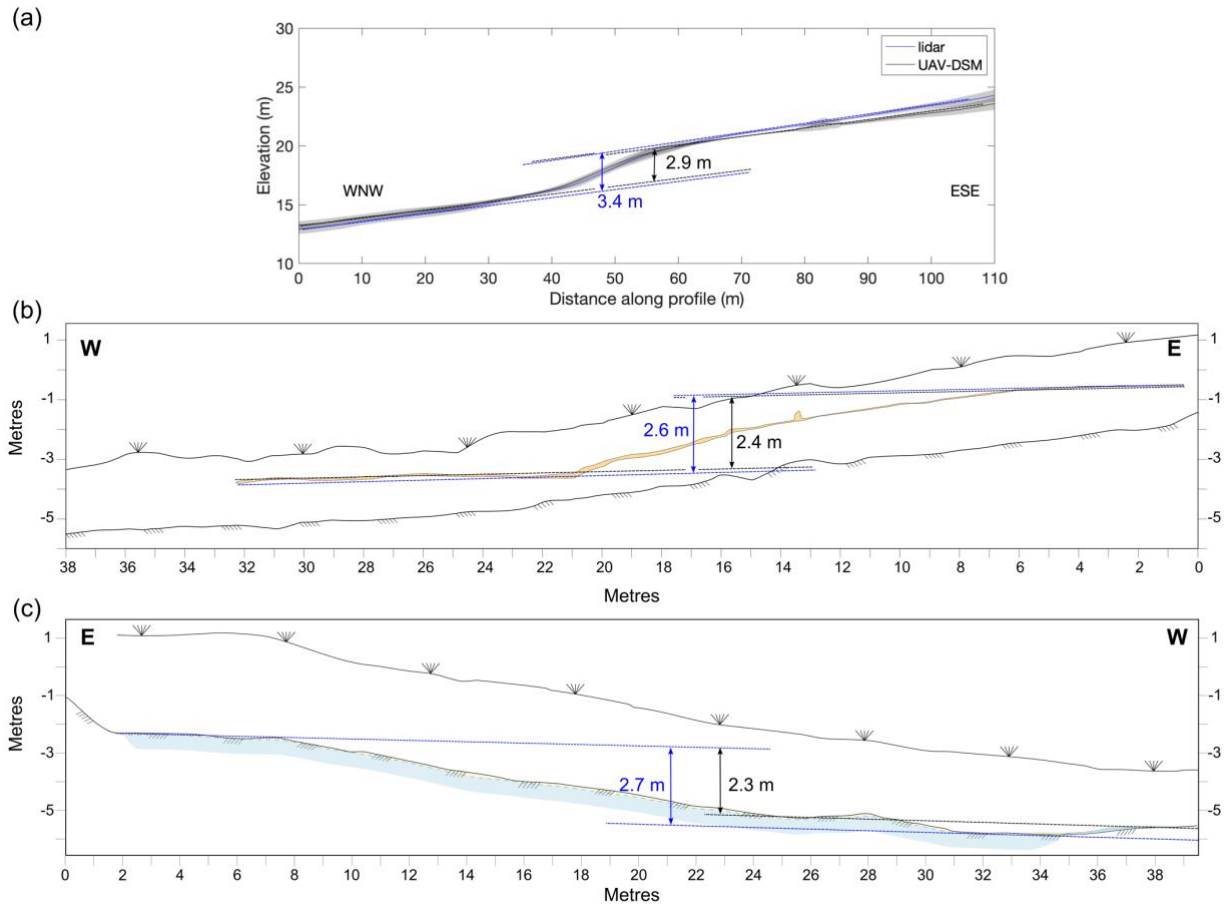

Figure S1: (a) Comparison of topographic profiles taken across the Owaka trench locality using a lidar digital elevation model and an Unmanned Aerial Vehicle (UAV) derived digital surface model (DSM). From each model, we plot the mean and standard deviation of elevation in 30 m wide swaths around the line indicated in Figure 8a in the main text, and then measure the vertical separation of regression surfaces either side of the scarp. (b&c) Vertical separation measurements obtained from the Owaka trench's stratigraphic units: (b) Unit 2c bed in the north wall (see Figure 10 in the main text for complete trench log) and (c) top of Unit 3 in the south wall (full trench log shown in Figure 9 in the main text). Black and blue regression lines represent minimum and maximum offset estimates respectively.

Figure S2

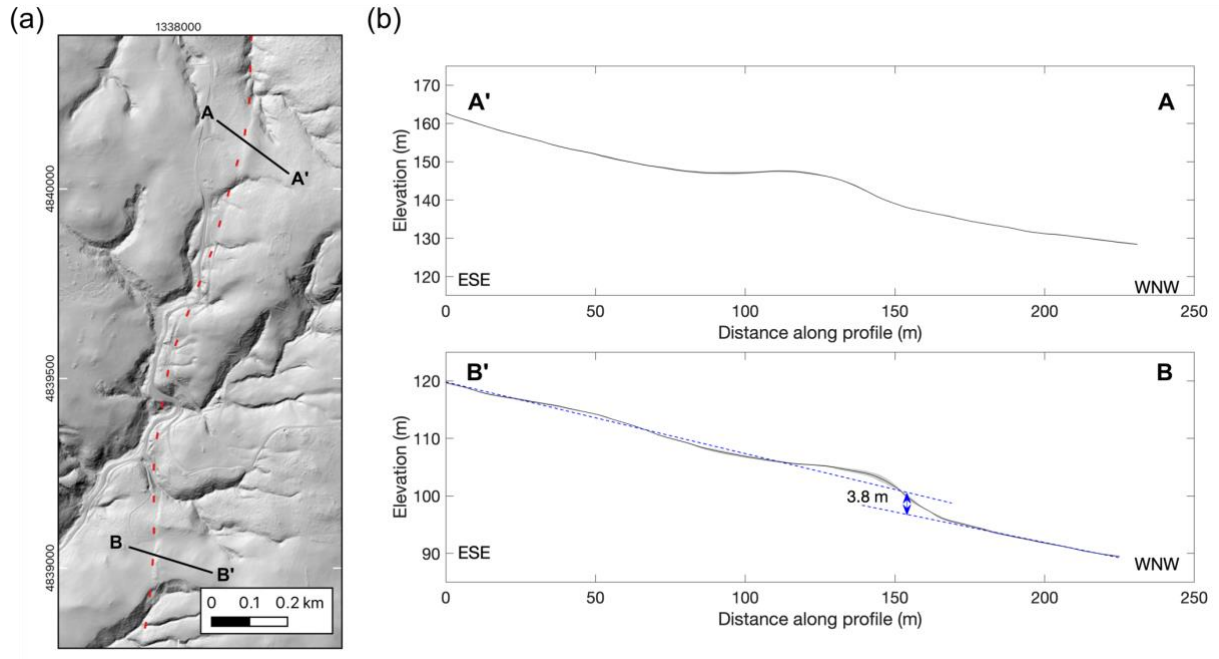

Figure S2: Lidar hillshade DEM of the Settlement Fault scarp (dashed red line) between Irahuka/Long Point and the Purakaunui River valley. Extent of (a) shown in Figure 2a in the main text. Coordinates in NZTM. (b) Topographic profiles in a 20 m wide swath across the Settlement Fault scarp from the lidar centred on the lines indicated in (a).

Figure S3

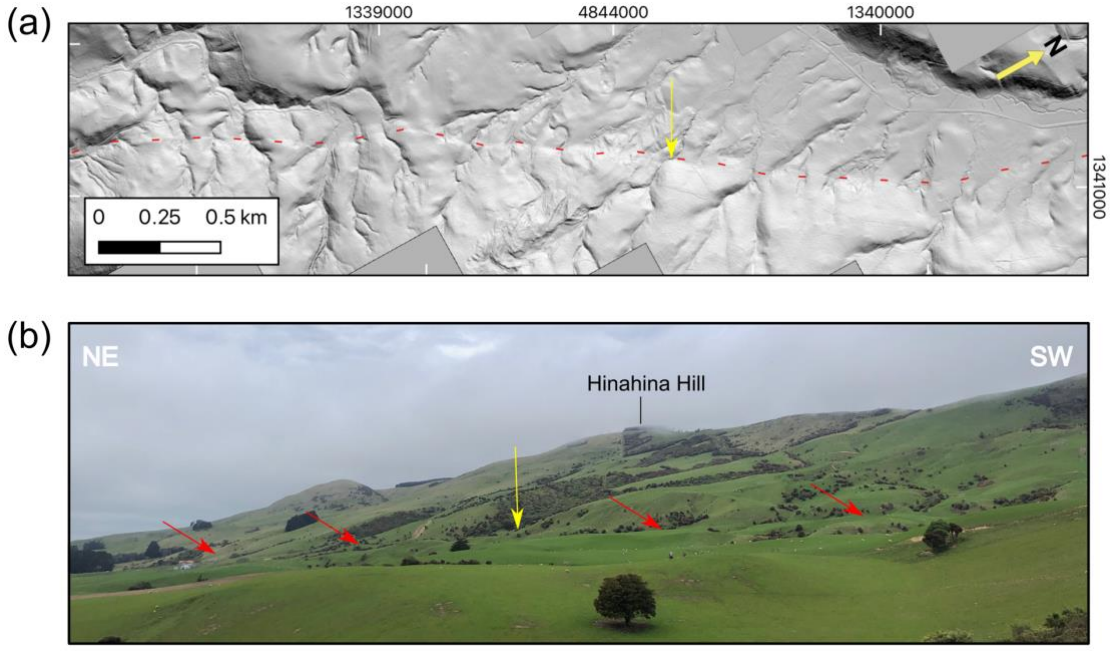

Figure S3: The Settlement Fault scarp inferred along the base of Hinahina Hill in (a) lidar hillshade DEM (dashed red line) and (b) field photo (red arrows). To help cross-reference the lidar map and photo, the yellow arrow in (a) & (b) indicate the same location. Extent of (a) shown in Figure 2a in the main text. Coordinates in NZTM.

Figure S4

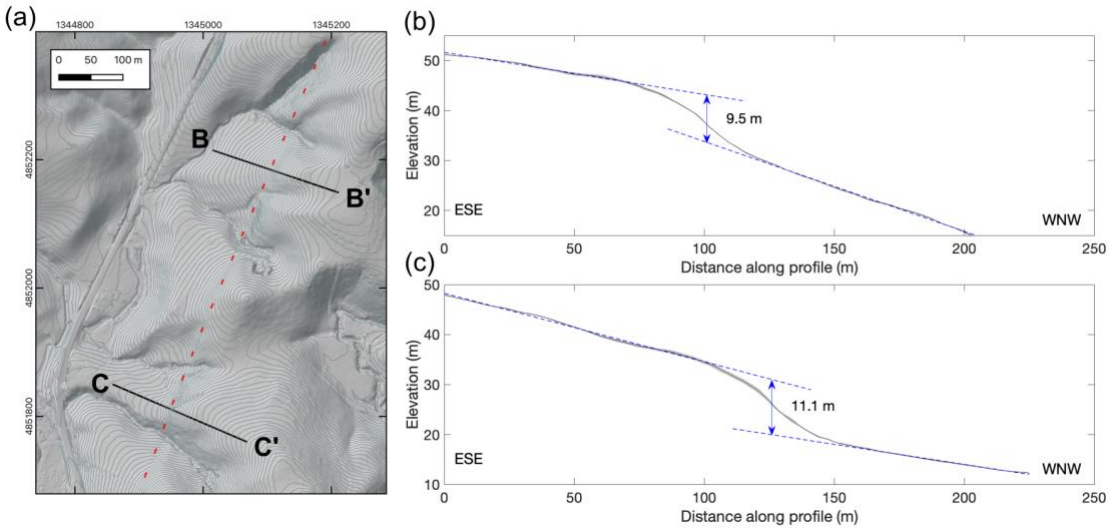

Figure S4: The Settlement Fault expression immediately north of the Owaka River. (a) Lidar hillshade DEM with fault trace (after Barrell 2021) indicated by dashed red line. 1-m-interval topographic contours were generated from lidar, and coordinates in NZTM. Extent of (a) indicated in Figure 2a in the main text. (b&c) Topographic profiles across the scarp generated from 20 m wide swath of lidar data centred on each profile line (for further description, see Methods section in the main text). These profiles highlight a broad topographic step at the location of the fault. The indicated ~10 m vertical displacement of the surrounding hill slopes is a maximum offset measurement, as these slopes are not parallel either side of the fault.

Figure S5

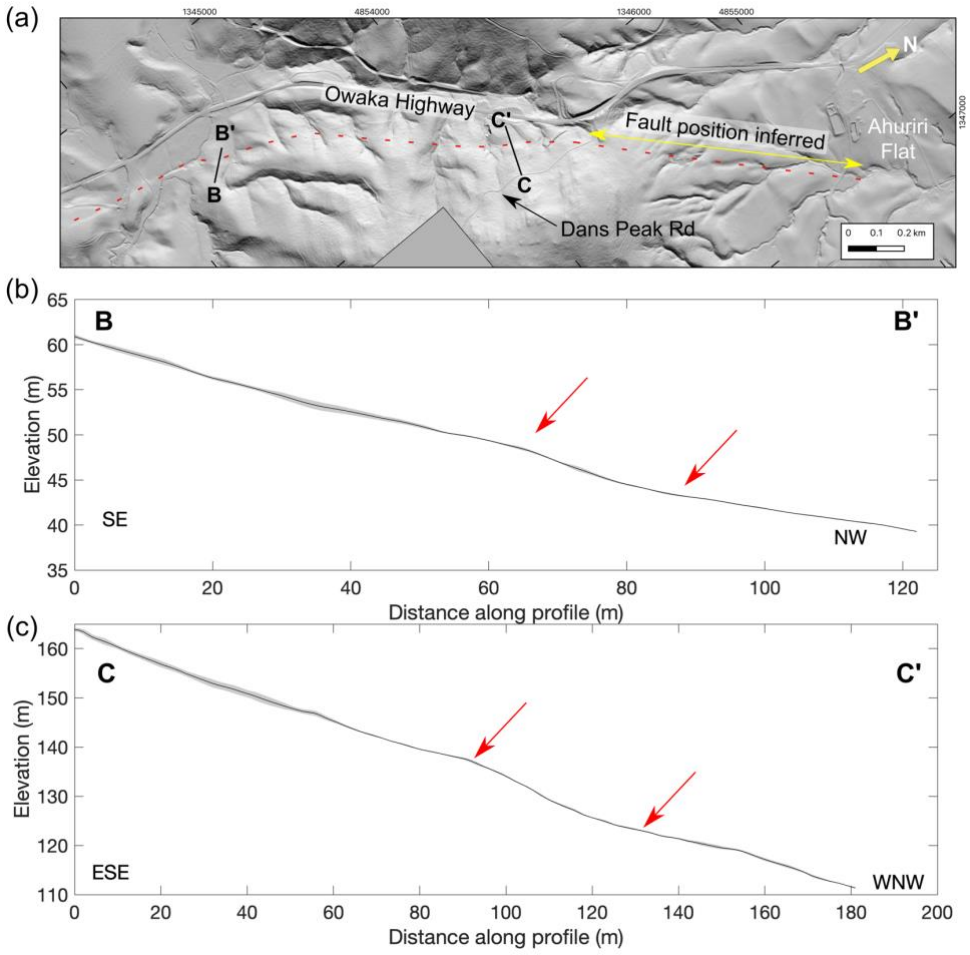

Figure S5: (a) A lidar hillshade DEM map at the Settlement Fault's northern end (dashed red line) around the Owaka Highway-Dans Peak Road junction. Extent of map shown in Figure 2a in the main text. (b&c) Topographic profiles from the lidar in 10 m wide swath centred on each profile line, and which highlight a broad topographic step at the location of the fault (as indicated by red arrows). Fault mapping after Barrell (2021).

Figure S6

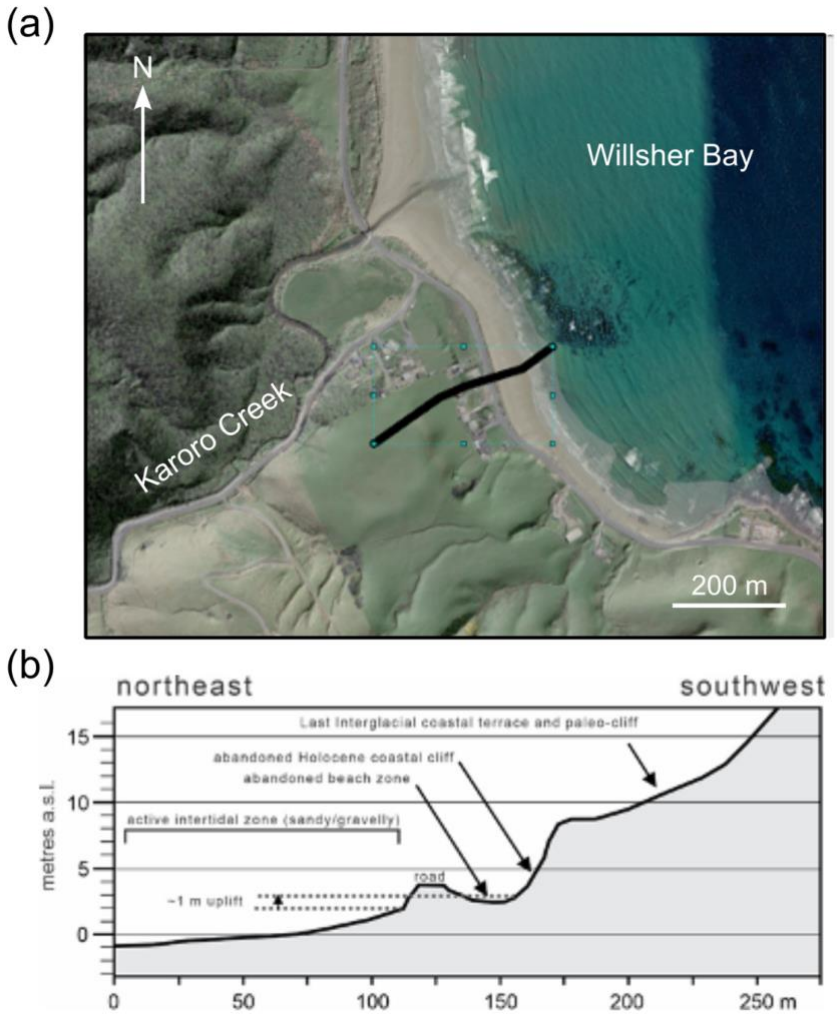

Figure S6: (a) Profile location and (b) annotated lidar profile at Willsher Bay where a possible uplifted Holocene coastal cliff that has been uplifted ~1 m is preserved. Location of (a) indicated by Figure 7 in the main text.

Figure S7

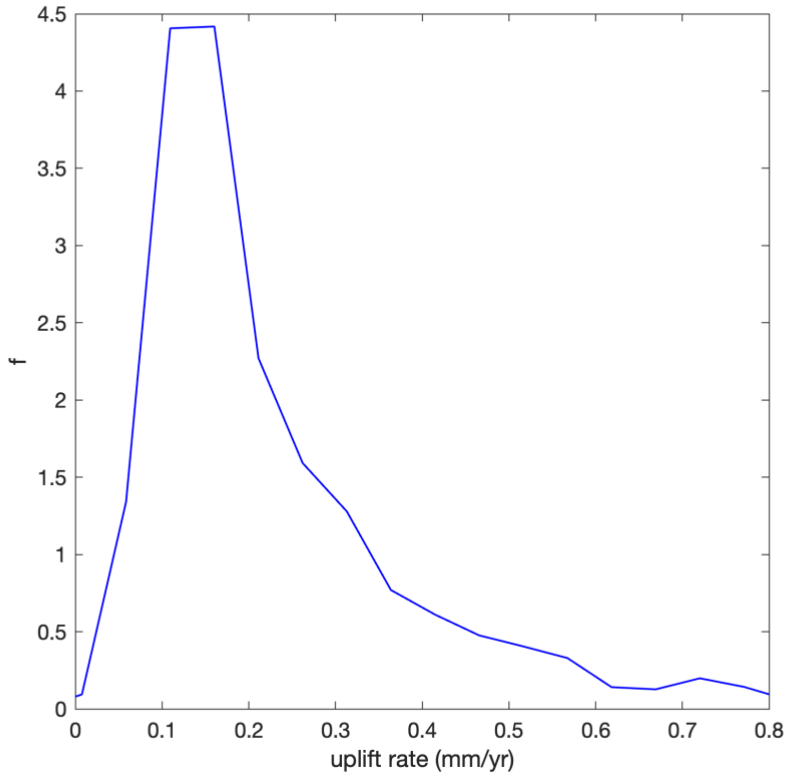

Figure S7: Kernel distribution functions for the short term Settlement Fault uplift rate estimate, as derived from repeating the slip rate calculation shown in Figure 12a in the main text for all 500 valid step sequences. Note, the distribution's positive skew.

Figure S8

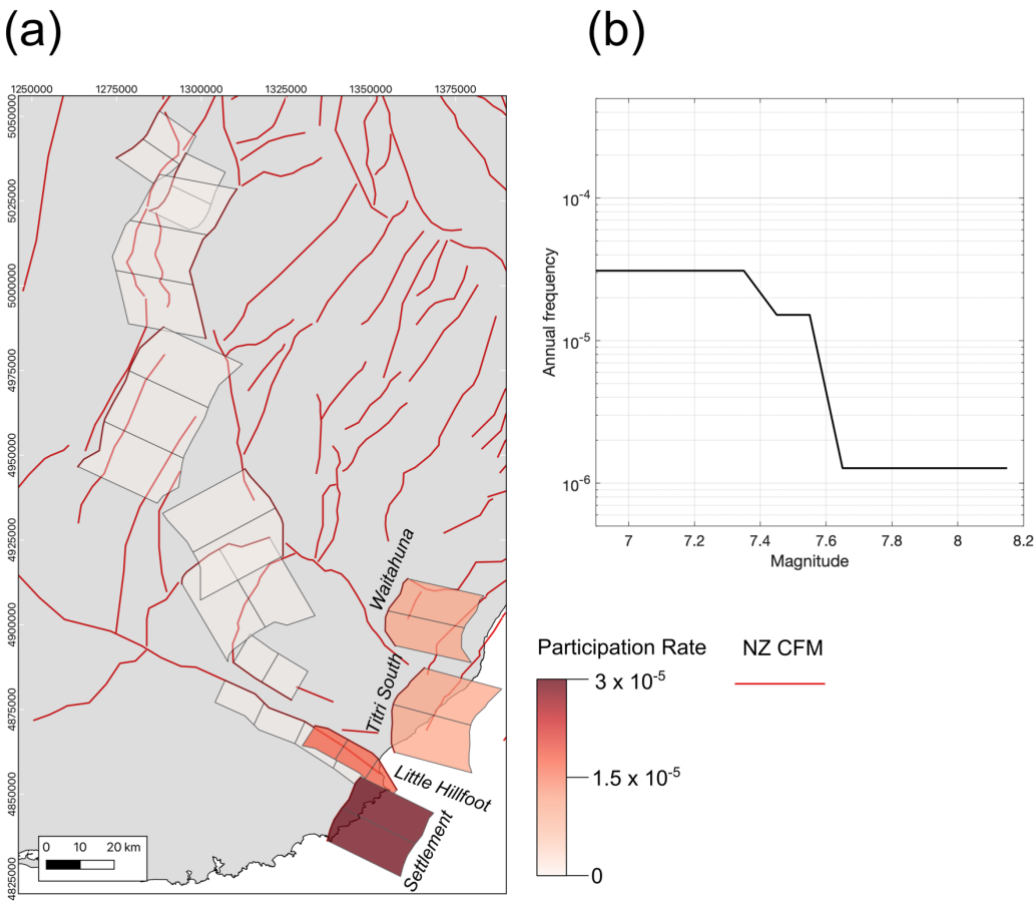

Figure S8: (a) Map of ruptures that the Settlement Fault participates in within the 2022 New Zealand National Seismic Hazard Model - Te Tauira Matapae Pūmate Rū i Aotearoa -Inversion Fault Model (NZ NSHM 2022 IFM; Gerstenberger et al. 2024). Each rupture patch indicates a discrete section, and the colour indicates the participation rate for that section's ruptures that include the Settlement Fault. The participation rates are derived from the weighted average of all rupture rates that are resolved from exploring the IFM logic tree branches. Red lines are other faults in the New Zealand Community Fault Model (NZ CFM; Seebeck et al. 2024). Note, this is not an exhaustive map of all multifault ruptures that the Settlement Fault may participate in, as the IFM solution does not utilize all plausible ruptures in the NZ NSHM 2022 rupture sets (Gerstenberger et al. 2024). (b) Magnitude frequency distribution of the ruptures that the Settlement Fault participates in the NZ NSHM 2022 IFM. Rupture geometry and rates as derived from: https://nshm.gns.cri.nz/RuptureMap (date last accessed 27/05/24).

References

Barrell DJA. 2021. General distributions and characteristics of active faults and folds in the Clutha and Dunedin City districts, Otago. GNS Science Consultancy Report 2020/88. 71 p.

Gerstenberger MC, Van Dissen R, Rollins C, Dicaprio C, Thingbaijim KKS, Bora S, Chamberlain C, Christophersen A, Coffey GL, Ellis SM, et al. 2024. The Seismicity Rate Model for the 2022 Aotearoa New Zealand National Seismic Hazard Model. Bulletin of the Seismological Society of America. 114(1):182–216. https://doi.org/10.1785/0120230165

Seebeck H, Van Dissen R, Litchfield N, Barnes PM, Nicol A, Langridge R, Barrell DJA, Villamor P, Ellis S, Rattenbury M, et al. 2024. The New Zealand Community Fault Model–version 1.0: an improved geological foundation for seismic hazard modelling. New Zealand Journal of Geology and Geophysics. 67((2)):209–229. https://doi.org/10.1080/00288306.2023.2181362

Supplement S2

Rafter Radiocarbon

Accelerator Mass Spectrometry Result

NZA 77218
R 41844/2
Job No: 223983
Report issued: 4 Aug 2023

Sample ID	OW-01-C02
Description	Charcoal fragments in sediments collected from paleoseismic trench wall
Fraction dated	Sediment
Submitter	Jack Williams Department of Geology, University of Otago

Conventional Radiocarbon Age	**Background**	±		(years BP)
$\delta^{13}C$ (‰)	-24.2	±	0.3	from IRMS
Fraction modern	0.0019	±	0.0007	
$\Delta^{14}C$ (‰) and collection date	-998.2	±	0.7	13 Feb 2023

Measurement Comment

This result is indistinguishable from 14C-free background materials prepared and measured concurrently with this sample. Therefore the reported fraction modern is a limiting age, not absolute.

Sample Treatment Details

136000 mg of raw sample was received. Description of sample when received: Sample was submitted in a plastic bag as charcoal fragments in brown/orange sediment. Broke apart sediment with scalpel and tweezers. Under the microscope were some fragmented pieces of charcoal/peaty material. The charcoal pieces were very fragile and covered in sediment; it was hard to remove sediment without breaking the charcoal pieces even more. Sample prepared by: Grind. Pretreatment description: Selected the crumbly, peaty material (no other dark, robust, organic material). Scraped off some of the sediment but not all of it as the material was very crumbly. After chemical noted under the microscope that the sample contained fine charcoal fragments and larger grey coloured balls of sediment. Removed as much sediment as possible before combustion. Chemical pretreatment was by acid, alkali, (which was repeated), acid. Weight obtained after chemical pretreatment was 19.1 mg. Carbon dioxide was generated by sealed tube combustion and 0.6 mgC was obtained. Sample carbon dioxide was converted to graphite by reduction with hydrogen over iron catalyst.

Conventional Radiocarbon Age and $\Delta^{14}C$ are reported as defined by Stuiver and Polach (*Radiocarbon 19*:355-363, 1977). $\Delta^{14}C$ is reported only if collection date was supplied and is decay corrected to that date. Fraction modern (F) is the blank corrected fraction modern normalized to $\delta^{13}C$ of -25‰, defined by Donahue et al. (*Radiocarbon*, *32*(2):135-142, 1990). $\delta^{13}C$ normalization is always performed using $\delta^{13}C$ measured by AMS, thus accounting for AMS fractionation. Although not used in the ^{14}C calculations, the environmental $\delta^{13}C$ measured offline by IRMS is reported if sufficient sample material was available. The reported errors comprise statistical errors in sample and standard determinations, combined in quadrature with a system error based on the analysis of an ongoing series of measurements of standard materials. Further details of pretreatment and analysis are available on request.

National Isotope Centre, GNS Science
PO Box 31-312 Lower Hutt, New Zealand Phone +64 4 570 4644
Email radiocarbon@gns.cri.nz Website www.RafterRadiocarbon.co.nz

Supplement S3

Report No. 6/23

Luminescence Dating Technical Report

Luminescence Dating Laboratory
School of Geography, Environment and Earth Sciences
Victoria University of Wellington
Wellington
New Zealand

Reported by: Ms. Ningsheng Wang
Date of Issue: 21-08-2023
Contact: Room 414
Cotton Building
Victoria University of Wellington
Ph: (04) 463 6127

CONTENTS

1. SUMMARY

Eight samples (Field code: PF23_OSL01 to PF23_OSL04 and OW_OSL01 to OW_OSL04) were submitted for luminescence dating by Prof. Mark Stirling, University of Otago. The laboratory codes of the samples are from WLL1587 to WLL1594 respectively.

The fine grain (4-11μm) preparation technique was used. Broadband luminescence was measured during infrared stimulation of fine-grained feldspar due to the absence of blue luminescence. The luminescence ages were determined by Single Aliquot Regenerative method (SAR). The dose rate was determined on the basis of gamma spectrometry measurements.

2. SAMPLE PREPARATION

The sample preparation consisted of two parts:

(i) Preparation for measurement of equivalent dose (equivalent to the paleodose)

(ii) Preparation for measurement of dose rate

Part 1: The Preparation for Measurement of Equivalent Dose (D_e)

1. Chemical Treatment

Samples had their outer surfaces removed. Of this removed outer scrapings, 100g was weighed and dried in an oven in preparation for gamma spectrometer analysis.
A plastic cube was then filled with remaining scrapings in preparation for water content measuring.

"Fresh" sample material, that had outer surfaces removed earlier (unexposed light sample material), was treated in 10% HCl. This was carried out overnight until all carbonate was removed by the reaction. Following this treatment, the sample was further reacted overnight with 10% H_2O_2 in order to remove organic matter.

The next step involved 200ml CBD* solution being added to the sample for 12 hours to remove iron oxide coatings. Note, after every chemical treatment procedure distilled water was used to wash the sample several times.

*CBD solution: 71g sodium citrate, 8.5 g sodium bicarbonate, and 2g sodium dithionate per litre of distilled water

2. Fine Grain Technique (4-11µm)

After chemical treatment, calgon solution (1g sodium hexametaphosphate per litre distilled water) was added to make thick slurry. This slurry was placed into an ultrasonic bath and mechanically agitated for an hour. The sample was then placed into a 1L measuring cylinder, filled with a certain amount of distilled water to separate out the 4-11µm grains according to Stokes' Law.

The 4-11µm grains were then rinsed with ethanol and acetone and a suspension of these grains were then deposited evenly onto 70 aluminium disks.

Part 2: The Preparation of Measurement of Dose Rate

The dry, ground and homogenised sample material were weighed and sealed in air tight perspex containers and stored for at least four weeks. This storage time minimizes the loss of the short lived noble gas ^{222} Rn and allows ^{226}Ra to reach equilibrium with its daughters ^{214} Pb and ^{214} Bi.

3. MEASUREMENTS

Luminescence age was determined by two factors: the equivalent dose (D_e) and the dose rate.

Equivalent dose: obtained from the lab equivalents to the paleodose absorbed by samples during the burial time in the natural environment since their last exposure to the light.
Dose rate: amount dose received by the sample each year.

Part 1: Determination of Equivalent Dose (D_e)

De was obtained by using SAR.

Single Aliquot Regenerative Method (SAR)

The Single Aliquot Regenerative Method (SAR) was used to determine the equivalent doses. This technique is described by Murray and Wintle (2000).

For the SAR method, a number of aliquots (disks) were subjected to a repetitive cycle of irradiation, preheating and measurement. Firstly, natural shining down curves was measured after preheating. Then shining down curves were measured for the next four or five cycles for different beta doses. Then from the variety of shining down curves, a luminescence growth curve (β induced luminescence versus added dose) was established. This was used to determine the equivalent dose (equivalent to the palaeodose). The measurement for the aliquots resulted in a variety of equivalent doses, so called dose distribution. D_e given in the report were used the arithmetic mean of the data.

In order to correct potential sensitivity changes from cycle to cycle, the luminescence response to a test dose was measured after preheat between cycles.

The broad band luminescence of 12 aliquots of each sample were measured at 50^0C for 100s using a Riso TL-DA-20 reader with infrared diodes at 880nm used to deliver a stimulated beam. Broad band luminescence from feldspar was then detected by an EMI 9235QA photomultiplier fixed behind two filters consisting of a Schott BG39 and L40. Beta irradiation was done on the Riso TL-DA-20 ^{90}Sr/Y β irradiator, calibrated against ^{60}Co gamma source, SFU, Vancouver, Canada with about 3% uncertainty. Preheat and cut heat temperature was 260 ^{o}C for 10 seconds.

Luminescence growth curve (β induced luminescence intensity versus added dose) was constructed by using the initial the first a few seconds of the shine down curves and subtracting the average of the last 20 seconds, along with the so called late light which was thought to be a mixture of background and hardly bleachable components. Interpolation of this growth curve to the dose axis was yielded the

equivalent dose D_e which was used as a paleodose. The measurements of 12 aliquots obtained 12 D_e's, the D_e's were accepted within 10% recycling ratio and max 10% recuperation rate. D_e used for the age determination was used the arithmetic means of the data. A dose recovery test and a zero dose were checked no anomalies.

a-value

a-value is measured by comparing the luminescence induced by alpha irradiation with that induced by beta or gamma irradiation. The a-value was for dose rate calculation.

Part 2: Determination of Dose Rate

Dose rate consisted of two parts.
(i) Dose rate from sample's burial environment
(ii) Dose rate from cosmic rays.

(i) *Dose rate from burial environment*

Dose rate from sample's burial environment was determined by radionuclide contents of ^{238}U, ^{232}Th and ^{40}K, a-value and water content.

Determination of Contents of U, Th and K by Gamma spectrometry

Gamma rays produced from sample material was counted for a minimum time of 24 hours by a high resolution and broad energy gamma spectrometer. The spectra were then analysed using GENIE2000 software. The contents of U, Th and K were obtained by comparison with standard samples. The dose rate calculation was based on the activity concentration of the nuclides ^{40} K, ^{208}Tl, ^{212}Pb, ^{228} Ac, ^{214} Bi, ^{214}Pb, ^{226} Ra, using dose rate conversion factors published by Guérin, G., Mercier, N., Adamiec, G. 2011.

Measurement of Water Contents

Water content was measured as weight of water divided by dry weight of the sample taking into account a 25% uncertainty.

(ii) ***Dose rate from cosmic rays***

Dose rate from cosmic rays were determined by the depth of sample below the surface along with its longitude, latitude and altitude, convention formula and factors published by Prescott, J.R. & Hutton, J.T. (1994).

4. RESULTS

Table 1 Cosmic dose rates

Table 2 Water contents, radionuclide contents

Table 3 a- Values, equivalent doses, dose rates and luminescence ages

Table 1: Cosmic Dose Rates

Laboratory Code	Depth Below the Surface(m)	Cosmic Dose Rate (Gy/ka)	Field Code
WLL1587	0.5	0.2051±0.0103	PF23_OSL01
WLL1588	0.5	0.2051±0.0103	PF23_OSL02
WLL1589	0.5	0.2051±0.0103	PF23_OSL03
WLL1590	0.5	0.2051±0.0103	PF23_OSL04
WLL1591	1.5	0.1694±0.0085	OW_OSL01
WLL1592	1.5	0.1694±0.0085	OW_OSL02
WLL1593	1.5	0.1694±0.0085	OW_OSL03
WLL1594	1.5	0.1694±0.0085	OW_OSL04

Table 2: Water Contents, Radionuclide Contents

Laboratory Code	Water Content (%)	U(ppm) from ^{234}Th	U(ppm) from ^{226}Ra, ^{214}Pb, ^{214} Bi	U(ppm) from ^{210}Pb	Th(ppm) From ^{208}Tl ^{212} Pb ^{228} Ac	K(%)	Field Code

WLL1587	5.7	1.08±0.21	1.12±0.11	0.87±0.17	4.02±0.07	0.62±0.01	PF23_OSL01
WLL1588	6.0	1.06±0.26	1.30±0.13	1.22±0.22	5.77±0.09	0.72±0.02	PF23_OSL02
WLL1589	4.4	1.24±0.24	1.14±0.12	0.93±0.20	4.92±0.08	0.83±0.02	PF23_OSL03
WLL1590	4.4	1.61±0.27	1.47±0.13	0.95±0.21	5.70±0.09	0.98±0.02	PF23_OSL04
WLL1591	21.4	2.67±0.23	2.44±0.14	2.74±0.23	9.74±0.12	2.01±0.04	OW_OSL01
WLL1592	21.1	3.04±0.33	2.46±0.15	2.36±0.24	9.63±0.13	1.99±0.04	OW_OSL02
WLL1593	24.5	3.87±0.41	2.98±0.18	3.12±0.29	12.06±0.15	2.43±0.05	OW_OSL03
WLL1594	31.2	3.09±0.36	2.58±0.17	1.84±0.25	10.78±0.14	2.01±0.04	OW_OSL04

Table 3: a-Values, Equivalent Doses, Dose Rates and Luminescence Ages

Laboratory Code	a-value	D_e(Gy)	Dose Rate(Gy/ka)	**Luminescence Age(ka)**	Field Code
WLL1587	0.095±0.018	41.39±1.21	1.90±0.03	**21.8±0.7**	PF23_OSL01
WLL1588	0.054±0.014	64.68±1.48	2.02±0.04	**32.0±1.0**	PF23_OSL02
WLL1589	0.083±0.006	25.22±2.62	2.20±0.03	**11.5±1.2**	PF23_OSL03
WLL1590	0.065±0.014	68.83±0.65	2.46±0.04	**28.0±0.5**	PF23_OSL04
WLL1591	0.066±0.012	66.85±1.01	3.63±0.11	**18.4±0.6**	OW_OSL01
WLL1592	0.050±0.004	64.96±0.43	3.45±0.11	**18.8±0.6**	OW_OSL02
WLL1593	0.051±0.004	78.95±0.47	4.07±0.15	**19.4±0.7**	OW_OSL03
WLL1594	0.044±0.003	73.07±0.48	3.23±0.14	**22.6±1.1**	OW_OSL04

5. REFERENCES

Guérin, G., Mercier, N., Adamiec, G. 2011: Dose- rate conversion factors: update. Ancient TL, Vol.29, No.1, 5-8.

Huntley, D.J. & Lamothe M.2001: Ubiquity of anomalous fading in K-feldspars and the measurement and correction for it in optical dating. Canadian Journal of Earth Sciences 38, 1093-1106.

Murray, A.S. & Wintle, A.G. 2000: Luminescence dating of quartz using an improved single aliquot regenerative dose protocol. Radiation Measurements 32, 57-73.

Prescott, J.R. & Hutton, J.T. 1994: Cosmic ray contributions to dose rates for luminescence and ESR dating: Large depths and long-term time variations. Radiation Measurements. Vol.23,Nos.2/3, 497-500.